A Reliable Protection Scheme for Fast DC Fault Clearance in a VSC-Based Meshed MTDC Grid

RIFAT ARA[1], (Student Member, IEEE), **UMER AMIR KHAN**[1], (Member, IEEE), **AAMIR IQBAL BHATTI**[1], (Senior Member, IEEE), AND **BANG WOOK LEE**[2], (Senior Member, IEEE)

[1]Department of Electrical Engineering, Capital University of Science and Technology, Islamabad 45750, Pakistan
[2]Department of Electronic Systems Engineering, Hanyang University, Ansan 15588, South Korea

Corresponding author: Umer Amir Khan (dr.umeramir@cust.edu.pk)

ABSTRACT A multi-terminal high voltage DC (MTDC) grid, is an optimum and cost-effective transmission network to minimize the energy crisis worldwide largely. However, the core demand for a fast DC protection scheme with an extraordinary strict fault clearance time of a few milliseconds, is a key research gap in this network, holding back its development and scalability. To bridge this gap, this paper proposes a novel protection scheme for a meshed MTDC grid. The main goals of the scheme include accurate discrimination of a faulty line, rapid fault detection, fault location estimation, significant fault current reduction, and fully selective isolation of only the faulted line, while continuing normal power flow in the healthy grid zones. Reliability of the scheme for long and extra-long-distance power transmission is increased by aiding the differential protection and Type-D traveling wave (TW)-based algorithms utilizing the distributed optical current sensing technology with the other auxiliary methods and backup plans. These auxiliary methods include independent discrete wavelet transform (DWT), current derivative polarity principles with a minimum sample (short time) window, overcurrent relays, and AC circuit breakers (ACCBs). A faulty segment of a transmission line is accurately discriminated from the healthy ones by measuring a series of multi-point differential currents on it. A faulty line at a particular DC node is accurately discriminated using the differential protection by measuring the current flowing into or out of each line from each side at every node to obtain the algebraic sum. The current sum of a real-time local transient data and a delayed remote data is compared to a preset threshold level. DC fault current is significantly reduced below the breakable levels by coordinating bidirectional hybrid DC circuit breakers (HDCCBs) with the active and passive fault current limiters (FCLs) and the half bridge-VSC-based modular multilevel converters (MMCs). The proposed concepts are successfully verified by the simulation results under a variety of fault scenarios and are found to be accurate.

INDEX TERMS MTDC grid, differential current protection, travelling wave-based fault location, fault detection, DC fault current limitation, faulty line isolation.

I. INTRODUCTION

In our modern society, to meet the fast-growing energy demands, tackle economic, technical, environmental concerns of conventional AC networks, deplete costly and vanishing fossil fuels, and prevent the effects of global warming, demand for a bulk integration of renewable energy in power networks is rapidly rising. The electricity cannot be stored but energy can be, and for the sustainable power supply, every kWh of the electricity needs to be utilized.

The associate editor coordinating the review of this manuscript and approving it for publication was Zhiyi Li.

Therefore, massive availability of power electronic devices, wide-band fiber optic tele-communication links, and use of the micro-computerized control units have made the HVDC transmission technology a powerful technology and facilitated the operation of an MTDC grid [1]. This Super-grid consisting of multiple sending and receiving terminals, incorporates the potential benefits of both the HVDC and HVAC systems. It is superior to conventional AC networks in economic, technical, and environmental aspects. It is a cost-effective transmission network with a bulk integration of renewable energy resources, especially offshore wind farms, solar, hydro, geothermal, etc.

It is basically built to transmit a bulk amount of sustainable electric power to long distances with the lower transmission losses, and overall lower investments saving land and money. Several benefits offered include more reliability, affordability, higher efficiency, secure electricity, access to large power markets through the international electricity trading, interconnection of weak and asynchronous AC systems, and possibility of connecting mainland networks to islands. The VSC-MMC-MTDC technology with a key benefit of constant voltage polarity, offers considerable benefits to fulfill the basic requirements of a large-scale meshed MTDC grid. This technology being a major enabler of the Super-grid, offers infinite extensions to the MTDC networks due to the implementation of extra-long hybrid transmission lines [1], [2]. However, the protection of DC systems is challenging and more difficult compared to AC systems protection. Major hurdles include the lack of high rating DC circuit breakers (DCCBs), absence of the naturally zero current crossings, minimum impedance in HVDC lines, absence of a standard protocol for HVDC networks, and grounding or corrosion issues in DC systems.

Therefore, high vulnerability of VSC-based HVDC systems to DC faults, particularly a solid DC line/cable short circuit or pole-pole (P2P) fault, with an extraordinary strict fault clearance time of a few milliseconds, has remained a core technical challenge in both research and practice so far. During this fault, even when all the IGBTs are blocked for self-protection, it is impossible to prevent the AC grid from feeding the fault, via the freewheeling diodes which form an uncontrolled bridge rectifier.

Therefore, in a meshed MTDC grid with multiple power sources and multiple lines or feeders per every node, all the devices and components experience large currents to feed the fault. As the number of line connections increases at a fault related DC node, the overall current interruption stress on the CB's of its faulted line increases accordingly. During the fault capacitive behavior, propagation delays of TWs, wave-front detection delays, synchronization delays, data processing delays, and interruption or isolation delays take place. The rate of rise of the short circuit fault current is extremely high, particularly when the fault is very close to a station (source). This fault is indeed, a worst-case fault scenario if it occurs very close to a remote source station. Since an MTDC grid feeds the fault, therefore, an accurate identification or isolation of only the faulty line or its faulty segment becomes impossible. If the fault is not cleared before the critical time limit, even the entire MTDC network will collapse.

Full-bridge fault blocking converters block AC infeed currents. However, their higher conduction losses and cost than the half-bridge converters, reduce their reliability in overhead transmission schemes. Indeed, converter protection strategies can fail in ring topology grids, due to the loss of selectivity and problems of restarting/ restoration after the fault [3]–[5]. Slow ACCBs, lacking both speed and selectivity are practically unsuccessful in a mesh type MTDC grid [6], [25].

Drawbacks of overcurrent protection such as lack of selectivity, sensitivity to load variations, and high impedance faults, make it unsuitable for a meshed MTDC grid [7], [8]. Importantly also, in a VSC-based MTDC grid, DC voltage polarity remains constant. Hence, the fault provoked DC link voltage transients (TWs) may give an estimation of the fault location in a TL, but cannot detect the wave-front [9]–[11].

Most drawbacks and challenges associated with the conventional differential protection and TW methods, can be eliminated with Type–D TW-based fault location and differential protection methods, utilizing the measurements obtained from the distributed optical sensors on hybrid transmission lines (HTLs) [12]. These optical schemes accurately discriminate a faulty segment, and require neither high sampling frequency nor accurate GPS time stamping. Optical sensor networks can be installed on any TL, regardless of the number of segments or sensors, as they are completely passive networks. Every optical sensor network operates independently and is not affected by the operation of any other sensing network. Off course, optical sensing technology can facilitate a high flexibility in the operation of a VSC-based MTDC network. Because a VSC-MTDC network implements the damage resistant cross-linked polyethylene (XLPE) cables of high mechanical strength, which are mostly buried except in the case of deep oceans. Therefore, in these cables, the reason for the fault is mostly due to mechanical damage. Technically, connection between the overhead lines (OHLs) and underground cables (UGCs), takes place at the ''transition joint pits'' where the actual onshore installations, current measurements, protective and control equipment's are realized.

Thus, in the VSC-based MTDC network, an optimum number of optical sensors can be equidistantly distributed on long TLs. Optical sensors can be installed around the transition joints, where the conductor connections take place and the current measurements are realized at these junctions. However, the reliability of these communication-dependent optical schemes is reduced for long and extra-long-distance power transmission. A communication-based fault discrimination/location algorithm, practically fails for the detection/location of a remote station close-up fault. Long overhead TLs passing through the complex terrains, and operating under harsh weather conditions, are often subjected to faults. Hence, a permanent tele-communication shut-down with a remote sensor/breaker failure is potential, which is a major cause of MTDC/HVDC outages. A worst-case close-up solid P2P fault at a remote station requires expensive backup plans. Continuous wavelet transform (CWT) is not suitable for quick fault detection in a non-stationary random signal with multiple peaks, as it consumes both time and memory space. CWT is more accurate in off-line fault location for which high speed is not required, except in the case of permanent short circuit faults [12], [13].

Most superior solution for reliable operation, integration, and extension of HVDC networks is to install the high rating DCCBs at DC line ends, to quickly isolate the faulty line.

Additionally, coordination of various types of DCCBs, FCLs, with the relay/sensor threshold settings, converter configurations, network topologies, and the fault detecting/ locating algorithms is extremely important to design a feasible MTDC protection scheme [14]–[16]. However, in the previous optical sensor schemes, there is no brief description about how to achieve coordination. Therefore, based on the existing literature, especially the optical sensor schemes [12], an alternate, comprehensive, cost-effective, robust, insensitive, and a fully selective DC protection scheme is proposed in this paper. It is applicable to medium and even large scale meshed MTDC grids, with several added benefits.

In the proposed scheme, an MTDC grid is protected from the DC faults by combining two ways. In one way, the overall DC fault clearance time is reduced, due to the accurate discrimination of the faulty line with fast fault detection, thus, allowing CBs to operate before the critical time. In the other way, the total DC fault clearance (grid outage) time is extended by significantly reducing the DC fault current to or below the breakable levels of available CBs. Thus, more reaction time is gained for both the fault detection and isolation. Rest of the paper is organized as follows: In Section II, theoretical analysis of the proposed scheme is described. Section III, describes the grid modelling. In Section IV, simulation results are discussed. Finally, in section V important conclusions are drawn based on the results of study.

II. PROPOSED PROTECTION STRATEGY

Primary goals of the work presented in this paper include all the important aspects as follows:

A. Accurate discrimination of a faulty line with the differential current algorithm based on distributed optical sensor measurements on transmission lines.

B. Rapid real-time detection of the wave-front arrival time utilizing independent DWT.

C. Significant reduction of the DC fault current below the breakable levels of hybrid DCCBs (HDCCBs).

D. Fully selective isolation of only the faulty line, instead of shutting down the entire MTDC grid.

E. Fault location in a TL, utilizing the current derivative data and TW- based methods.

A VSC-based MTDC grid, requires less communication between its converter stations. Although the controllers at the stations are identical in design, but they work independent of each other (independently control both the active and reactive powers). Thus, the reliability of communication-dependent differential protection and Type-D travelling wave methods based on the distributed optical sensor networks as in [12], for long/ extra-long-distance power transmission is increased by aiding them with auxiliary independent and simple backup plans. These auxiliary schemes include the current derivative polarity principles, discrete wavelet transform (DWT), active and passive FCLs, simple overcurrent protection, ACCBs, and other backup options.
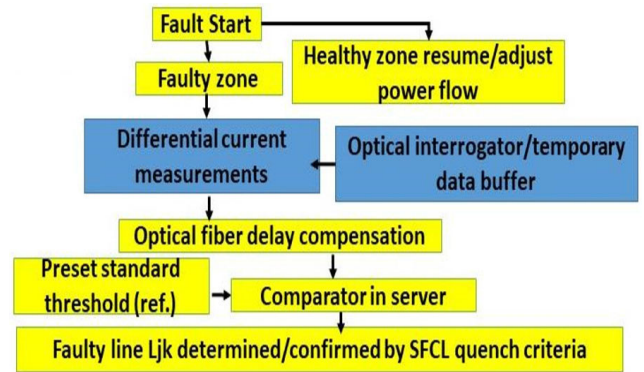

FIGURE 1. Faulty line or segment discrimination flow chart.

A. FAULTED LINE DISCRIMINATION

A meshed MTDC grid with MMC_j and MMC_k as the number of terminals, has $I_{jk}(j, k = 1, 2, 3, 4 \ldots, N)$ DC currents measured at each terminal respectively (see Fig. 5). DC current measuring units (assumed as the optical sensors) S_1 to S_n were distributed on all the cables. Each cable consists of m segments ($m = 1, 2, \ldots, n - 1$). P2P faults were simulated in the cable L_{12}, while P2G faults were simulated in the cable L_{13} respectively. Accurate identification of the faulty line with fast fault detection, shortens the overall fault clearance time. Differential protection algorithm seems to be very promising in the protection of an MTDC grid, as it is highly selective in discriminating and normally operates faster (within 2 ∼ 5 ms). Therefore, it can coordinate well with the proactive nature of a hybrid DCCB (constant breaking time of 2 ∼ 3 ms) and works well with very small inductors. Both the source and load terminals are considered and three ways are explored to determine a faulty line or its faulty segment as follows:

1) DETERMINATION OF A FAULTY LINE BETWEEN TWO SOURCES

Flow chart for accurate determination of a faulty line is shown in Fig. 1. Since an MTDC grid feeds the fault, and causes the current to flow from all locations in the direction of the fault, therefore, the basis used is the differential protection combined with the current derivative polarity principles. DC current flowing into or out of the cable from each side at every node (both the fault related and non-related) is measured to obtain the algebraic sum and a precise, large enough threshold is set to accurately identify the faulty line.

Thus, a faulty line L_{jk} b/w the two source nodes B_j and B_K of Fig. 5, is accurately discriminated by measuring the current flowing out of or into every DC cable from each side at every node to obtain the algebraic sum. The current sum is the sum of the real-time local transient data, and a history data of the remote measurement.

Thus, the current sum measured at B_j at the time of t_0, is the sum of the current I_{jk} flowing out of B_j measured locally at the real-time of t_0, and the current I_{kj} flowing out of B_k and into

the cable L_{jk} measured at τ before t_0 or vice versa. Similar current sums on both sides of every cable at buses B_1 to B_4 were measured respectively. Since the input signals are the local current and the remote line current, therefore, due to the distributed optical sensor measuring arrangement on the TLs, there is no need of accurate GPS time stamping between the two signals. Importantly also, measurement of the differential current sums at every node, not only discriminates a faulty line, but also its faulty segment. Therefore, this method of measurement is faster than the series method as in [12]. Since the algorithm relies on the optical sensor communication link b/w the two-line ends, therefore, continuous data transfer with bidirectional communication only during the fault events, can greatly relax the speed need for long distance power transmission. Measuring differential current sums at every node, along with the Type-D TW-based method, requires a smaller number of equidistantly distributed optical sensors (usually one sensor installed around the transition joint).

This further aids in achieving the cost effectiveness of the scheme. Thus, the differential current sum on the faulted cable L_{jk} is given in equation (1).

$$U_{jk}(t_0) = I_{jk}(t_0) + I_{kj}(t_0 - \tau)$$
$$U_{kj}(t_0) = I_{jk}(t_0 - \tau) + I_{kj}(t_0) \qquad (1)$$

The differential current sum obtained is then compared to a preset and large positive threshold valu I_{dTH+} such that

$$U_{jk}(t_0) > I_{dTH+} \times I_{nom} \qquad (2)$$

Let the absolute values of the current sums U_{12}, U_{13} and U_{14} measured at the source node B_1(Fig. 5) are the elements of a row vector such that:

$$U = [U_{12(peak)}, U_{13(peak)}, U_{14(peak)}] \qquad (3)$$

In order to discriminate a faulty line L_{12} from the healthy ones at B_1, verify the highest peak such that:

$$[M, I] = \max(U) \qquad (4)$$

where M is the highest peak of the differential current sum derived from the faulty line L_{12}, and I is the index value at that peak respectively.

2) DETERMINATION OF A FAULTED LINE B/W A SOURCE AND A LOAD TERMINAL

Sum of currents entering or leaving a node is zero during normal operation according to the KCL. However, the fault in a charged power line, splits the line current between the load and the fault currents. Let us take MMC_j as a source terminal and MMC_k, as a load terminal. The faulty line L_{jk} between them is accurately discriminated by measuring the difference of two currents at its each end as in equation (6). Consider the positive current flow in the cable L_{12} from the source MMC_1 terminal to the load MMC_2 terminal in Fig.5. For an internal fault within the protection zone of the cable L_{12}, the events that occur are:

$$\Delta I_a = \Delta I_{F12} + \Delta I_b \quad or \ \Delta I_{F12} = \Delta I_a - \Delta I_b \qquad (5)$$

$$I_{diff} = I_{Ljk(in)} - I_{Ljk(out)} \qquad (6)$$
$$I_{diff} = I_{line/seg(in)} - I_{line/seg(out)} \qquad (7)$$

3) DETERMINATION OF A FAULTY SEGMENT

For a non-homogeneous TL consisting of m number of segments with n number of series optical sensors distributed along it, a faulty segment of it is accurately discriminated from the healthy ones, by measuring a series of differential currents between every adjacent sensor pair S_m and S_{m+1}. Constant communication delay τ is determined using the speed of TWs and the distance b/w the adjacent sensors S_m and S_{m+1} respectively such that:

$$I_{diffm}(t_0) = i_{sm}(t_0) - i_{sm+1}(t_0 - \tau) \qquad (8)$$

where $I_{diffm}(t_0)$ is the m-th differential current derived from the two adjacent sensors Sm and S$m+1$ ($m = 1, 2, \ldots, n - 1$). For external faults outside the protection zone of line L_{12} or its faulty segment, the differential current is very close to zero, while for an internal fault a highest value of differential current is derived. In terms of the current derivative or the rate of change of current, τ_w is a short time (a minimum sample) window selected.

$$= di_{sm}(t_0)/dt - di_{sm+1}(t_0 - \tau_w)/dt \qquad (9)$$

B. FAST FAULT DETECTION

Fig. 2, illustrates the flowchart for real-time detection of the fault generated surge arrival time. Here the optical sensor data is periodically collected in a run-time input temporary buffer (an Optical Interrogator). Then the collected sensor data from the buffer is transmitted to a computer server, to permanently maintain all the sensor readings in a database for further analysis and coordination. The sensor data in the server can be remotely or wirelessly queried by an operator in order to collect the results/issues/updates if required and interact with the available resources to direct the necessary actions to be taken. At the same time the remote operator can also manage the operation of the entire transmission system by interacting with the maintenance plans.
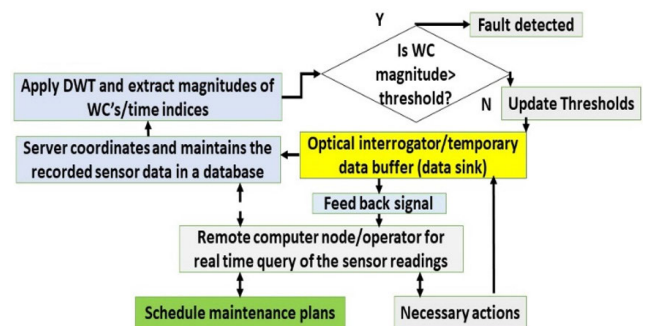

FIGURE 2. Flowchart for rapid fault detection using DWT (DSP).

Fault provoked current transients (TWs) are reflected forward and backward b/w the terminals and the fault point, causing multiple peaks (stepwise increase) in the fault current development like a staircase waveform. During testing, when

the distance to the fault *Df* was 1 ∼ 10 km, the fault current exhibited a clear TW effect when zoomed in and rose sharply making the critical time much shorter. Since the independent DWT is a digitalized WT, therefore, it is more practical in detecting the wave-front arrival time in real time non-stationary signals with multiple peaks. DWT with less computational burden and de-noising applications, is locally applied to every node in a meshed grid. This allows each terminal to independently identify its faulty line using simple local DC current measurements in a relatively short time.

Thus, there is no need of inter-terminal or tele-communication, and correct tripping of even remote CBs becomes possible. In DWT, an input signal is decomposed into different output levels called the wavelet coefficients (WCs) or scales with the help of an analyzing function called the mother wavelet (MW). The corresponding WC is compared to a preset threshold level for the fault detection.

Precise and large threshold settings (much above the noise level), and the selection of a correct MW that has the closest (best) match with the fault current pattern, are the key requirements in the WT, to avoid wrong fault detection and false tripping. Some key features of the DWT include automatic window size adjustment as per the signal dynamics and simultaneous time and frequency localization capabilities. Insensitivity of the DWT coefficient to noise and other disturbances, distinguishes the DC side fault from the AC side faults and load changes, so that a reasonable robustness is achieved. The higher the absolute value of a WC, the closer the chosen MW matches to the fault current pattern. In the HVDC systems, compact MWs of high frequency such as '*Haar- 6*' and '*db1-4*', are suitable for the fault detection. They perform better to localize the high frequencies in the fault current transients, with a minimum delay of around 1 ms. Consistently high WC's of the faulty line currents and low WC's of the healthy line currents, help to distinguish between the internal and external faults respectively..

C. PROPOSED FAULT CURRENT LIMITATION

FCLs are inserted on either AC or DC side to effectively reduce the fault current, thus allowing longer reaction time for both the fault detection and isolation. Usually DC side FCLs limit the fault current magnitude in Stage 1 (DC capacitor discharge stage) and Stage 2 (diode freewheel stage) of the DC cable short circuit fault. AC side FCLs limit infeed AC currents in Stage 3 (grid current feeding stage) of the fault response. However, neither the inductors on DC side nor the FCLs on AC side, alone can effectively protect the system from the DC faults. Stage-2 is the most challenging stage, in which the IGBT modules are blocked shortly by self-overcurrent protection as soon as the fault current starts to exceed a threshold level of about twice the nominal value [7]. The blocking condition of a half-bridge converter is when the arm current exceeds about 1.8 p.u. (w. r. t. peak arm current), and the conduction by all diode arms begins at this instant. Therefore, even after installing the FCLs on AC side of the converters, the destroying overshoot current at

the beginning of Stage 2 still exists, and forces the weakest diodes to pass a huge current with a high initial value through them. This puts the diodes and the cables at a high risk. Indeed, Stages 1 & 2 are the most stringent periods to take the fault decision (trigger the IGBT block signal within 2 ms). Any FCL and interruption device increases the total grid impedance, and slows down the dynamics of the system. Therefore, increasing the size of protective inductors leads to increase in total impedance of Stage 3, which causes decrease in the maximum DC cable current [17].

Thus, various drawbacks of large-sized and extra inductors include increased grid inductance and time constant of the system, more reactive power losses, inductive kickback effects, voltage instability, increased mass and volume of a converter station, and increased cost [12], [19]. Therefore, the single-ended methods can practically fail to locate the fault in a TL [18], [19]. Indeed, if the inductor size is increased to a very large value, the diode current would eventually drop with the decrease in total cable current which is highly unwanted. A non-linear resistor such as a superconducting FCL (R-SFCL) being passive, does not affect to the systems transient response. However, its drawbacks of the recovery time in seconds (>1s), large quenching impedance, higher power consumption and energy dissipation, larger size, and high cost are highly unwanted in an MTDC grid [20], [21].

Now during testing, RSFCLs effectively limited the DC cable short circuit current when installed on the DC side. Since an arm overcurrent criterion is used to block the IGBTs of a VSC, therefore, the Rectifier (source) IGBTs will block earlier than those of an Inverter. Thus, in the proposed scheme, large and extra inductors are avoided. A communication-based fault discrimination algorithm is coordinated with bidirectional HDCCBs, small inductors of 15 ∼ 50 mH, R-SFCLs, half bridge VSC-based MMCs, ACCBs, and the other passive components to compromise with the cost and size of the network components. Utilizing the potential benefits of both the inductors and R-SFCLs, the DC fault current is significantly reduced to or below the breakable levels of a HDCCB. Properly sized series inductors (one per pole) are added at the DC output of only AC/DC converter stations to allow continuous operation of the grid without converter blocking during and after the fault. These inductors limit AC side contribution to the fault current. In order to design a proper size of an inductor, important parameters which were taken into consideration include contributions from the weak, medium strong, and very strong AC sources to the DC fault current, rated AC and DC voltages, rated power, peak currents on the healthy and faulty cables, current ratio, and the current limiting effects of inductors and RSFCLs.

D. FAULT CURRENT INTERRUPTION AND ISOLATION

Fig. 3, illustrates the flowchart for fully selective isolation of only the faulty line. Since, only the R-SFCLs located on the faulty line will quench and limit the fault current.
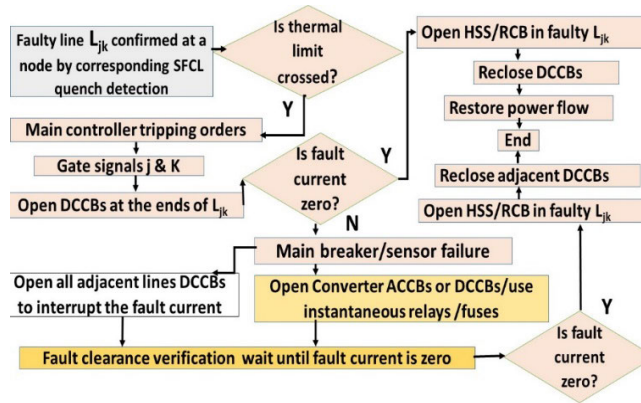
FIGURE 3. Fully selective methodology to isolate only the faulted line with backup plans in an MTDC grid.

FIGURE 4. Flowchart for the fault location in a transmission line.

Thus, a communication-based fault discrimination algorithm, confirms the faulty line among multiple lines at a fault related node, depending on the quench detection of the associated R-SFCL. In equation (6), the controller monitors the difference of two currents in the faulty line L_{jk}. As soon as the difference exceeds a preset, and large threshold level and the faulted line L_{jk} is confirmed based on the quench detection of the associated R-SFCL, the controller sends tripping orders to the concerned HDCCBs at both the ends of L_{jk} to interrupt the fault current, and isolate only it, while resuming normal power flow in the healthy grid zones. Thus, a HDCCB opens to interrupt the fault current only when the associated R-SFCL quenches.

An R-SFCL helps to selectively isolate a faulty line, eliminates the chances of false tripping/triggering, reduces the electrical stress on the other FCU components, and helps to quickly perform a backup option if required. For a faulty line both the HDCCBs are opened, while for a healthy line only one HDCCB is tripped if necessary. Thus, the time constraint is made less strict in HVDC systems. If in equation (3) among the differential current sums U_{12} U_{13}, and U_{14}, both U_{12} and U_{14} have a positive sign (ascending behavior), and the sign of sum U_{13} is negative (decreasing behavior) or zero, then among the current sums U_{12} and U_{14}, the HDCCB that exhibits the highest magnitude of the sum is opened, while the other HDCCBs at B_1 remain closed. The HDCCB through which the current sum does not surpass either of (+/-) thresholds, remains closed.

E. FAULT LOCATION IN A TRANSMISSION LINE

Fig. 4, shows the flowchart to locate the fault in a TL. The current derivative data or WC data obtained during the fault detection, is used with TW methods to determine the arrival time of the wave-front, and locate the fault in a TL. The sensor data obtained during the fault detection, is processed offline by using CWT with either '*Haar*' or '*db*' MWs to locate the fault in a TL. Distance of a converter station/ sensor to the fault location '*Df*' in a TL, is one of the key factors affecting to the rate of rise of the DC fault current derivative and DC
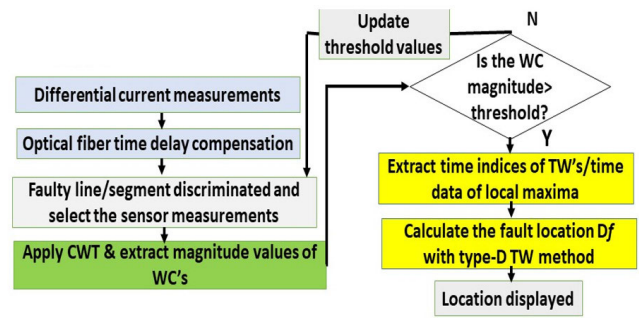
voltage transients, and hence, is an important parameter to locate the fault in a TL.

Because the closer a station and or/sensor is to the fault point, the higher the magnitude of the fault current derivative and its corresponding WC gets. Indeed, the highest interruption DC fault current occurred for a solid P2P fault in the cable L_{12} at 1 km to the source node *B1*.

When the fault occurs extremely close to a station's node (1 ∼ 5 km), the current derivative surpasses the threshold level quickly and makes the critical time much shorter. However, as '*Df*' increases, magnitude of the fault current derivative and its corresponding WC decreases (damping occurs). Thus, due to the attenuating effect of long TLs on the fault current transients, it is impossible to locate a remote station close up fault. Now, if the current derivative direction method with a short time (a minimum sample) window and precise threshold settings, is combined with the differential protection and Type-D TW-methods, utilizing the optical sensor communication links, the current derivative method performs much better to locate the fault and even reduces the communication errors.

Additionally, the influence of different distances to a solid P2P fault on the fault induced DC voltage transients was tested. DC voltage sharply dropped to or very near to zero, for a solid P2P fault at 1 ∼ 13 km to the node/measuring unit, and the TW effect was not clearly visible in such cases. However, as the distance '*Df*' increased, DC voltage also increased above the zero level, thus indicating the nearness (closeness) of a converter station/sensor to the fault point. Therefore, the DC link voltage transients can fail to detect the wave-front arrival time, particularly for a solid close-up P2P fault to a station or sensor [9]–[11]. However, DC voltage transients can be used to estimate the fault location in a TL.

III. GRID MODELING

Initially, the tests were carried with mono-polar, bi-polar 2-level, and 3-level VSC-HVDC links 300 km ∼600 km long and AC voltages were varied from 230 ∼ 800 kV. Nominal AC power/frequency of 4 ∼ 10 GVA/60 ∼ 50 Hz, line-end inductances of 10 ∼ 15 mH, and DC side capacitors up to 120 μF were used. Then the 3-level, bi-polar half-bridge VSC-MMC-MTDC meshed grids of 3 and 4 terminals were
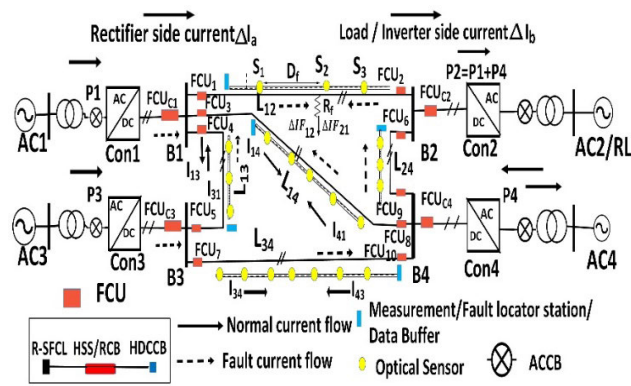
FIGURE 5. A four-terminal meshed MTDC grid with optical sensor networks, fault locators and protection devices.

TABLE 1. Simulation parameters.

S.no.	Parameters	Value
1.	AC Voltage and AC Frequency	230 kV to 800 kV, 50 to 60 Hz
2.	DC-side Caps, Resistive-load, Line-Reactors, Power Consumption, Nominal Current	10-200 μF,150 Ω-200 MΩ,10-15 mH (for two terminal links only, bipolar/mono -polar/2level/3level), 500 MW, 2 kA
3.	DC Voltage, DC Bus Capacitors (1/node)	up to ± 860 kV, 10-120 μF
4.	DC-Cables(L12/L13/L14/L34/ L24/L32)	180 km -600 km/120 km/300 km/180 km/90 km/300 km
5.	Series Inductor 2/ (AC/DC) or source converter output (active current limiting)	10 mH – 70 mH
6.	R-SFCL (passive current limiting) 4/DC cable, 2/converter if needed	min R_{SFCL} = 0.01 Ω to max 25 Ω, trigger I_q = 3 kA
7.	AC Transformer Leakage Reactance	0.15 p.u. to 0.2 p.u.
8.	R_f, D_f (Fault)	0 Ω-500 Ω, 1 km-600 km
9.	FCU 4/line &2/Converter	HDCCB, operation 2 ms, breaking capability up to 9 kA
10.	Converter Technology	Half-bridge 3-level -VSC-MMC
11	Converter Blocking (dip/trip), Threshold detection point	2.5-2.9 kA (blocking condition Arm current exceeds 1.8 p. u)

tested as shown in Fig. 5. Current measuring units were distributed on the π-section DC cables. The fault clearing units (FCUs) were inserted as 4/cable (2 for each pole) and 2/converter (1 for each pole). An FCU consists of a bidirectional HDCCB combined with R-SFCL and high-speed switch (HSS)/ RCB [20]. R-SFCL quenches after the fault and passively limits the fault current. Four DC bus capacitors of $5 \sim 50$ μF (1/ node) were added to accelerate the quenching of the SFCLs due to the discharge currents.

System parameters used are listed in the table-1. For continuous operation of the grid, properly sized series inductances of $15 \sim 50$ mH (2/converter) were added at the DC output of AC/DC converter stations (1 for each pole) to limit
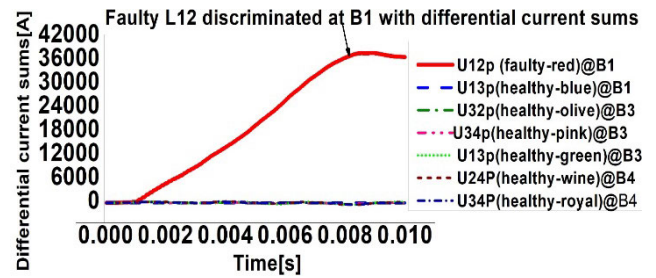

FIGURE 6. A Faulty line L_{12} (red-solid curve) discriminated at B_1 by measuring the differential current sums without protection.

the rate of rise of AC infeed currents, and therefore, avoid the converter blocking. Discharge from every healthy DC cable was passively limited by two R-SFCLs. Four ACCBs were inserted on the AC sides of converters to increase the reliability of the scheme.

IV. SIMULATION RESULTS
A. FAULTY LINE AND FAULTY SEGMENT DETERMINATION RESULTS

In Fig. 6, a faulty line L_{12} 300 km long, was accurately discriminated from the healthy ones, for a solid P2P fault at 1 ms between S_1 (B_1) at 10 km and S_2 at 40 km to the fault by measuring the differential current sums on each cable connected to the nodes B_1 to B_4 in a meshed 4-terminal grid. The other cable lengths were cable L_{13} of 120 km, L_{32} of 300 km, L_{34} of 180 km, and L_{24} of 90 km respectively. Table 2 lists the values and for a solid P2P fault at 1 km to B_1, highest peak (25 kA) of the current sum is seen. In Fig. 7, a faulty segment of the cable L_{12} (180 km long) was accurately discriminated for a solid P2P fault at 1ms b/w S_1 at 1 km and S_2 at 29 km to the fault by measuring a series of differential currents on it. Seven sensors were distributed on the cable L_{12} with 30km separation b/w each adjacent pair. In Fig. 5, due to a P2P fault b/w the pair S_1 and S_2, current reversal takes place through them as shown in Fig. 8. Thus, for an internal fault within the protection zone of the line L_{12}, I_a the rectifier side current through S_1 ascends, and I_b, the inverter side current through S_2 descends. This also indicates the partial discrimination property of the current derivative direction method when used alone, and hence, can be used as a back-up plan [25], [26].

B. FAULT DETECTION RESULTS
In Fig. 10, using DWT, suddenly a high WC is registered for a solid P2P fault b/w S_1 at 10 km and S_2 at 20 km to the fault in the cable L_{12}, before installing the FCU's (without protection). The fault is shortly detected at 270th sample value using 'Haar -6' as the MW and WC's are almost zero before and after the fault. The smaller the fault impedance R_f value, the larger the fault current magnitude (shorter the critical time), and vice versa. In order to detect a high resistance P2P fault in the cable L_{12}, R_f was increased from $0.01 \sim 500$ Ω. Magnitude of both the fault current and

TABLE 2. Maxi. I- Sums at DC buses with different D_f to P2P fault.

D_f from B1	1km	10km	150km	198km
i_sumL12(+) @B1(faulty)	25 kA 7.7ms	22 kA 8.24ms	13.1 kA 9.3ms	10.6 kA 10ms
i_sumL32(+) @B2(healthy)	684 A 2ms	674 A 1.1ms	487 A 2.71ms	1500 A 2.26ms
i_sumL13(+) @B1(healthy)	1 kA 1.3ms	435 A 1.6ms	389 A 1.71ms	400 A 1.57ms
i_sumL13(+) @B3(healthy)	856 A 6.5ms	861 A 1.51ms	1 kA 4.4ms	1 kA 4.26ms
i_sumL32(+) @B3(healthy)	717 A 1.8ms	718 A 2.01ms	794 A 2.3ms	659 A 1.9ms
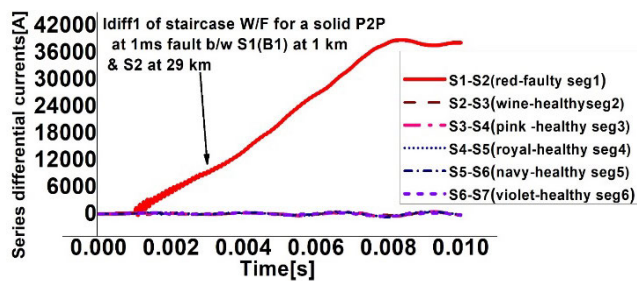
FIGURE 7. A Faulty segment (red-solid curve) of L_{12} discriminated by measuring a series of differential currents on it without protection.
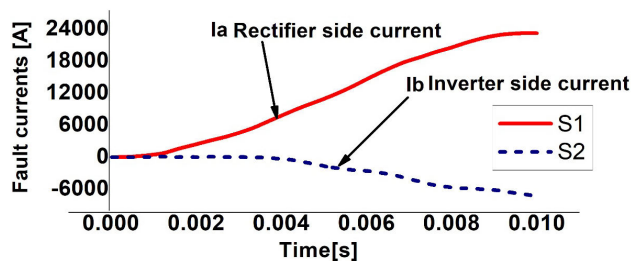
FIGURE 8. Current reversal b/w S_1 and S_2 oriented for the positive current flow from the sending MMC$_1$ to the receiving MMC$_2$ terminal due to an internal mid-line P2P fault in the cable L_{12} without protection.

its WC decreased due to the damping effect of large R_f as shown in Fig. 9 and Fig.11 respectively. In Fig. 9 with a series of differential current measurements, it is impossible to discriminate a faulty segment (red-solid curve) from the healthy ones initially, due to the damping effect of large R_f. However, in Fig. 11 using DWT, indeed, the WC magnitude reduced greatly with protection and using R_f of 500 Ω. But even then, the WC magnitude remained well above the WC's of the healthy cable currents and threshold level, therefore, clearly discriminating a faulty segment/line from the healthy ones. Fig. 12, shows the detection of a near solid P2P fault at 10 km to source node B_1 (red-solid curve). Table 3 lists the detailed WC magnitudes, indicating the closeness of a P2P fault in the cable L_{12} to the fault related nodes B_1 and B_2.
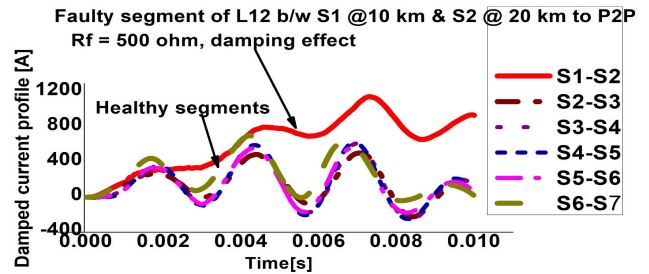

FIGURE 9. Damped profile of series differential currents for $R_f = 500\Omega$ without protection.
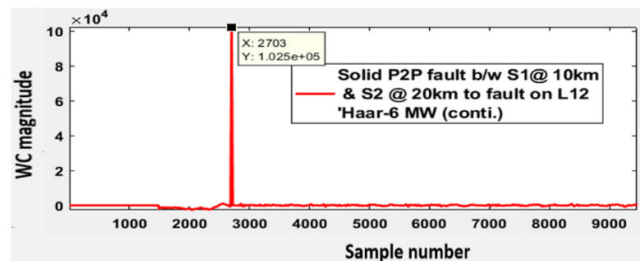

FIGURE 10. Suddenly a high WC 'd6' registered for a solid P2P fault b/w S_1 at 10 km and S_2 at 20 km to fault in L_{12}. The fault is shortly detected at 270th sample value with Haar-6 as the MW without protection.
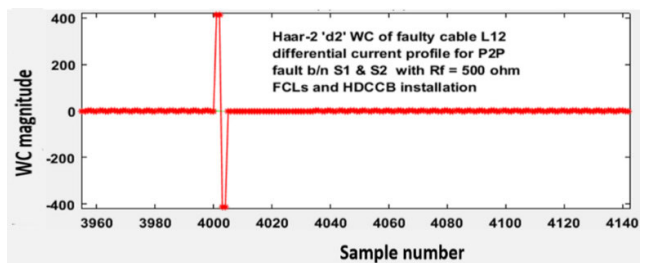

FIGURE 11. With protection after installing FCU's and using $R_f = 500\Omega$ WC on the faulty cable reduced greatly but its value stayed well above the WC's of the healthy cable currents and threshold levels.
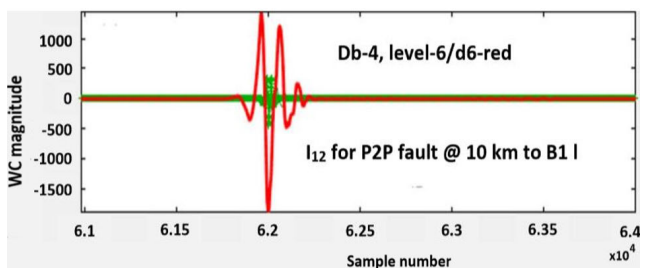

FIGURE 12. A Solid P2P fault at 10 km to $B1$ in the cable L_{12} (600km long) generates a high WC 'd6' (red-solid curve). WCs are almost zero before & after the fault. WC's of a damped transient are shown by green-solid curve.

C. EFFECTIVE DC FAULT CURRENT LIMITATION RESULTS

In the literature so far, DC fault current is limited to around $3 \sim 4$ kA, however, at the expense of large sized and extra inductors. To practically verify this, DC fault current was reduced to 3.387 kA by inserting 200 mH inductors, 4/ each

TABLE 3. Detailed WC magnitudes with Haar-3 MW.

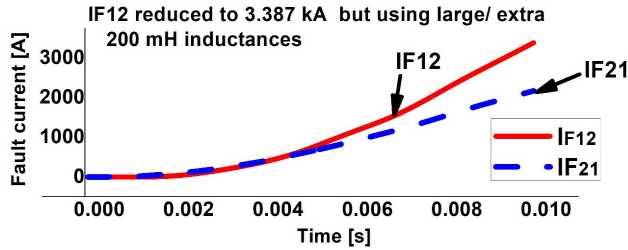| D_f to B1	10km	100km	180km	199km
B1(faulty)	135.3	39.56	46.07	40.55
B2(faulty)	21.38	38.07	55.62	512.3
B3(healthy)	1.21	2.39	4.972	8.809
B4(healthy)	0.8176	1.599	6.07	8.78

FIGURE 13. DC fault current limited to 3.387 kA with extra inductors of 200 mH 4/each cable and 2/each converter in a meshed MTDC grid.
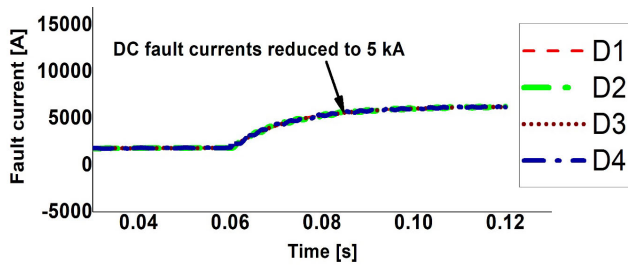

FIGURE 14. Fault current reduced to 5 kA with 30 mH inductors at the DC outputs of only AC/DC converters with protection in the scheme.
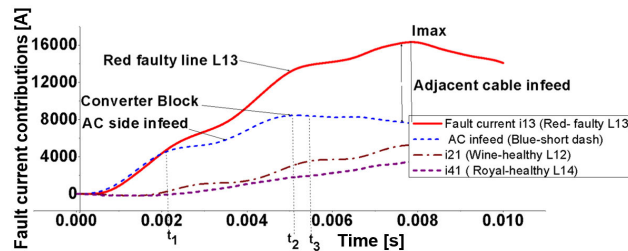
FIGURE 15. Total contributions to the fault current for a P2G fault in L_{13} at 1 km to B_1 without protection. Faulty cable L_{13} current (solid red curve), MMC_1 DC current (blue short dash) and healthy cable currents (wine and royal).

DC cable and 2/each converter in a meshed 4-terminal grid as shown in Fig. 13. However, with the proposed scheme, the DC fault current was significantly reduced from huge values to around 5 kA ~1.7 kA, by adding series inductors of 10 ~ 50 mH at the DC output of only AC/DC converter stations (2/converter) as shown in Fig. 14, Fig. 20, and Fig. 22. Fig. 15, shows the total contributions to the DC fault current for a P2G fault at 0.5 ms in the cable L_{13} and at 1 km to node B_1.

The current rise rate through the FCU_4 (Fig. 5) is highest (red solid curve). During the period b/w $t_1 \cong 2.3$ ms and $t_2 \cong 5.24$ ms, major contribution to the fault current is the
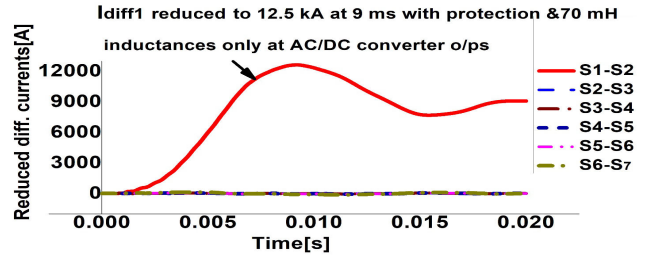

FIGURE 16. Huge differential current derived from the faulted pair S_1 and S_2 of Fig. 7 is reduced to 12.6 kA with protection in the scheme.
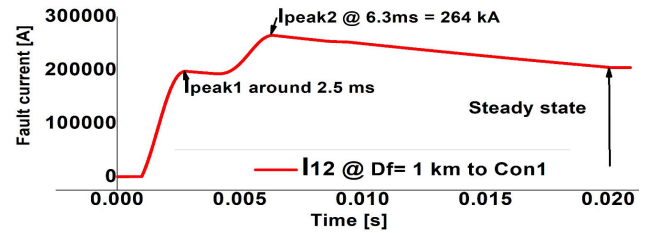

FIGURE 17. Huge P2P fault current with strong AC sources (800 kV).

AC infeed via MMC_1. MMC_1 side arm current decays from t_2 onwards, however, the current through the faulty cable L_{13} keeps on increasing. This is because after the converter blocks at time t_2, currents through the adjacent healthy cables L_{12} (wine-dash-dot) and L_{14} (royal–dash) are significant from t_2 onwards due to prominent discharges. If the current breaking capability for the HDCCB at the converter output is increased up to the maximum fault current contribution from one converter, then the R-SFCLs (2/converter) placed at the converter output could be omitted. If the rated line current is 2 kA, then the R-SFCL quenching current is $I_q = 1.5 \sim 3\times$ line rated = 3 kA. Current to be limited is:

$$I_{cable} < I_{\lim} < I_q \qquad (10)$$

For $I_q = 3 \times 2$ kA = 6 kA, Fig. 20 and Fig. 22, satisfy equation (10) criterion, i.e. 2 kA < 4.8 kA< 6 kA. R-SFCL is modeled as a generic–type DC SFCL considering the four parameters, such as response time of 2 ms, a minimum impedance of 0.01 Ω during the normal operation, which jumps to a maximum value of 20 $\sim$ 25 Ω at the fault instants, and triggering current of 3 kA.

D. FAULT CURRENT INTERRUPTION AND ISOLATION RESULTS

Fig. 17, shows the timely development of a huge fault current through the $HDCCB_1$ for a solid P2P fault in the cable L_{12} at 1 ms and at 1 km to B_1. Both the terminals 1 and 2 were very strong AC power sources of 800 kV with the nominal power/ frequency of 10 GVA/60 Hz in a 2-level bipolar 3-terminal grid. There are two peaks visible clearly, one at 2.5 ms and the other at 6.3 ms. During the first 2.5 ms, fault current pattern is determined by the DC capacitor discharges and the current surges (Stage 1). In Stage 3, the AC contribution keeps on
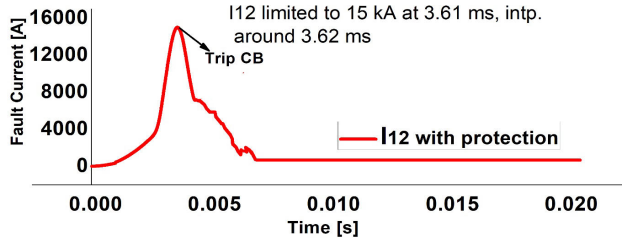
FIGURE 18. Fault is isolated at around 5.2 ms with protection.

TABLE 4. Type A & D fault location methods with $R_F = 0.01\,\Omega$.

Distance D_f (type A)	10km	30km	100km
Estimated distances(km)	9.8901	29.7	98.97
Absolute Error (km)	0.1099	0.3	1.03
Distance D_f (type D)	10km	30km	100km
Estimated distances(km)	9.976	30.88	100
Absolute Error (km)	0.024	-0.88	0

increasing and recharges the DC capacitor (capacitors) until the peak arrives. After this discharging into the fault takes place, and the maximum $HDCCB_1$ current I_{peak2} is arrived at 6.3 ms. Gradually the DC capacitor contribution decreases until the steady-state at around 20 ms arrives.

The DC capacitor is still charged and discharged in the steady-state, but without any contribution to the fault current. In Fig. 18 with protection, at around 3.62 ms, $HDCCB_1$ and $HDCCB_2$ are tripped to interrupt the DC fault current and isolate the faulty cable L_{12} at around 5.2 ms. The time elapsed b/w the fault trigger at 1 ms and the CB tripping at 3.62 ms is 2.62 ms. In order to limit the fault current within the acceptable levels, it should be interrupted in less than 20 ms [23]. Theoretically a DC protection scheme with the total fault clearance time of up to 5.1 ms. is regarded as a fast scheme. Hence, the proposed scheme with $t_{total} = 5.12 \sim 5.28$ ms can be deemed as a fast scheme.

E. FAULT LOCATION RESULTS

To locate the fault in the cable L_{12} (180 km long) using the current derivative data, first seven sensors were distributed on it with 30 km separation between each adjacent pair. A solid P2P fault was triggered at 0.5 ms b/w S_1 at 10 km and S_2 at 20 km to the fault for a simulation time of 1.5 ms. A short time window of information selected was 0.76 ms ($t_1 = 0.669$ ms and $t_2 = 0.76$ ms) with an estimated distance of 9.702 km.

For a P2P fault at 0.2 ms b/w S_1 and S_2 with simulation time of 5 ms and a minimum window of 0.6 ms ($t_1 = 0.3$ ms and $t_2 = 0.6$ ms), the estimated distance was 29.7 km. Then the cable L_{12} of 200 km length was tested for a solid P2P fault at 10 km to B_1. A minimum window of information selected was 0.1866 ms ($t_1 = 0.0867$ ms and $t_2 = 0.1866$ ms) with an estimated distance of 9.8901 km using Type-A travelling wave-based fault location method. Then Type-D TW-based
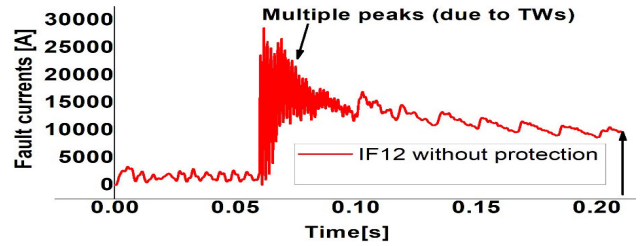

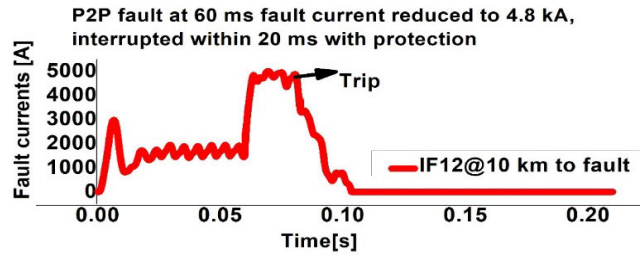**FIGURE 19.** DC fault current with multiple peaks without protection.

FIGURE 20. DC Fault current effectively limited to 4.8 kA, interrupted and isolated within a short time with protection.
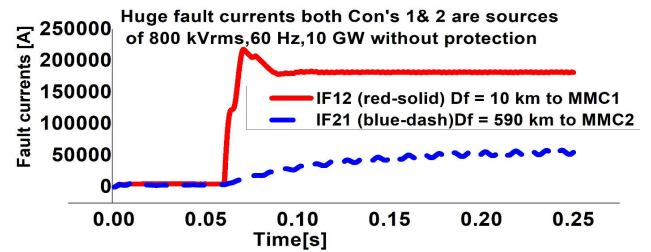

FIGURE 21. Influence of different distances to a solid P2P fault on DC fault current transients showing the damped transient (blue dash).

method was tested and table 4 lists some of the results. According to Type-A method:

$$D_f = (t_2 - t_1) \times v/2 = t_{mea} = (t_2 - t_1) = 2D_f/v$$
$$v = c/\sqrt{\varepsilon_r} = c/n = 1/\sqrt{LC} = 3 \times 10^5 (\text{km/s})/\sqrt{2.3}$$
$$= 198\text{km/ms} \quad (11)$$

where t_1 and t_2 are the arrival times of the first two TWs to reach to a terminal (sensor). If $D_f = 50$ km to B_1 on the cable L_{12} which is 300 km long, then the total distance covered is 100km such that $t_{mea} = 0.5$ ms. Total delay as in [19] is

$$t_{total} = t_{CB} + t_{mea} + t_{process} \quad (12)$$

If $t_{process} = 1$ ms, $t_{mea} = 0.5$ ms and $t_{CB} = 2$ ms, then $t_{total} = 3.5$ ms. As shown in Fig. 18, $t_{CB} = 3.62$ ms, $t_{total} = 5.12$ ms, therefore, again the proposed scheme can be deemed as a fast scheme. According to the Type-D TW-based fault location method.

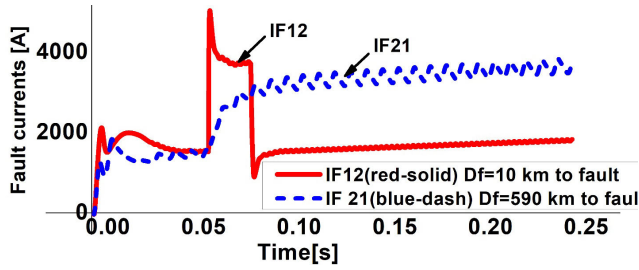$$D_f = L_{seg} - \tau(t_{S1} - t_{S2}) \times v/2 = L - (T_j - T_K) \times v/2 \quad (13)$$

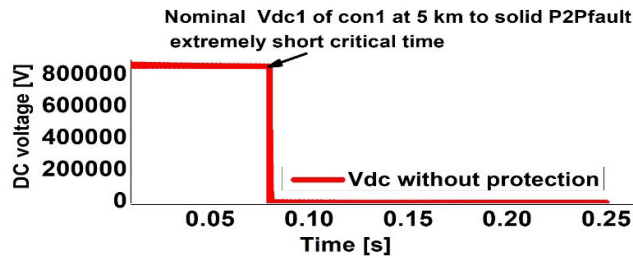**FIGURE 22.** DC fault currents with protection.

FIGURE 23. HVDC link voltage without protection for a solid P2P fault at a distance of 5 km to the source node B_1 (MMC_1).
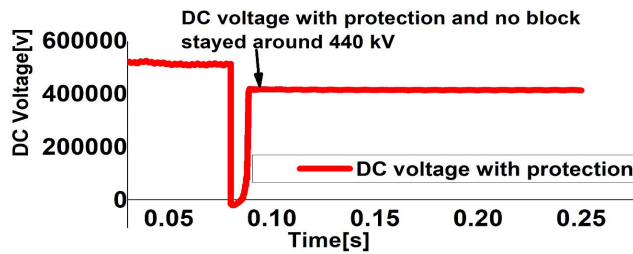

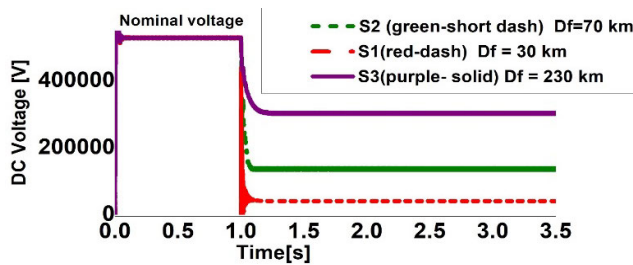**FIGURE 24.** HVDC link voltage with protection and no block.

FIGURE 25. Influence of varied distances to a solid P2P fault on HVDC link voltage transients without protection.

In Fig. 21, as the distance of MMC_2 increases from the fault location, attenuation (damping) occurs in the fault current I_{F21} (blue-dash curve). With the proposed protection, these huge fault currents are limited, interrupted, and the faulty line L_{12} is isolated within a short time as in Fig 22. Fig. 25 and Fig. 26, shows the influence of different distances of sensors to a solid P2P fault in the cable L_{12} on the DC voltage transients. As the distance of a sensor to the fault location increases, the corresponding DC voltage transient also increases. Also damping oscillations are seen in the voltage transients of the faulty line L_{12} due to the TW effects
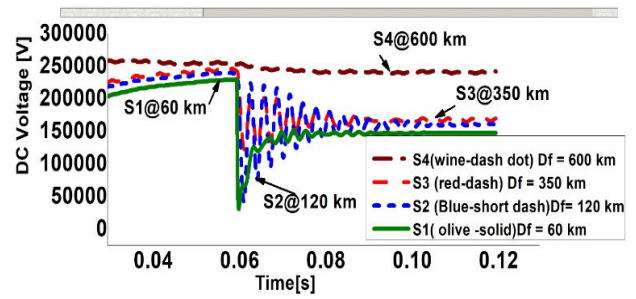

FIGURE 26. Influence of varied distances to a solid P2P fault on the HVDC link voltage transients. Damped oscillations due to TWs without protection in the faulty line.

as in Fig. 26. A solid P2P fault was simulated in the cable L_{12} at a distance of $1 \sim 5$ km from the source node B_1 as shown in Fig. 23 and Fig. 17. Table 4 lists results of fault locations estimated with both Type-A and Type-D fault location methods.

V. CONCLUSION

This paper proposes a fully selective HVDC protection scheme, which enables quick fault detection, faulted line discrimination and identification, fault current limiting, and fast and accurate isolation of the faulted line. The presented algorithm utilizes the differential protection and travelling wave fault location methods based on the optical sensor networks for long/extra-long-distance power transmission lines. Discrete Wavelet Transform is used for the fault detection. If the Wavelet Transform becomes less effective to detect the fault, alternate simple back-up plans like instantaneous overcurrent relays, SFCL quench criteria with a communication-based algorithm and current derivative principles are used. DC fault current is significantly reduced below the breakable levels by coordinating bidirectional hybrid DC circuit breakers (HDC-CBs) with the active and passive fault current limiters (FCLs) and the half bridge-VSC-based modular multilevel converters (MMCs). The proposed concepts are verified by the simulation results under a variety of fault scenarios, and are found to be accurate. Further, expensive back-up plans are avoided. Future work includes rigorous analysis on the backup plans, and verification of the proposed algorithm on RTDS systems for an MTDC grid.

REFERENCES

[1] H. Dong, Z. Xu, P. Song, G. Tang, Q. Xu, and L. Sun, "Optimized power redistribution of offshore wind farms integrated VSC-MTDC transmissions after onshore converter outage," *IEEE Trans. Ind. Electron.*, vol. 64, no. 11, pp. 8948–8958, Nov. 2017.

[2] G. Zhang, Z. Li, B. Zhang, and W. A. Halang, "Power electronics converters: Past, present, and future," *Renew. Sustain. Energy Rev.*, vol. 81, no. 2, pp. 2028–2044, Jan. 2018.

[3] D. Tzelepis, A. O. Rousis, A. Dyśko, C. Booth, and G. Strbac, "A new fault-ride-through strategy for MTDC networks incorporating wind farms and modular multi-level converters," *Int. J. Electr. Power Energy Syst.*, vol. 92, pp. 104–113, Nov. 2017.

[4] C. Petino, F. Schettler, D. Eichhoff, M. Stumpe, M. Heidemann, and E. Spahic, "Application of multilevel full bridge converters in HVDC multiterminal systems," *IET Power Electron.*, vol. 9, no. 2, pp. 297–304, Feb. 2016.

[5] Q. Song, S. Xu, Y. Zhou, Y. Gim, Z. Li, and Z. Deng, "Active fault-clearing on long-distance overhead lines using a hybrid modular multilevel converter," in *Proc. IEEE 28th Int. Symp. Ind. Electron. (ISIE)*, Jun. 2019, pp. 2033–2038, doi: 10.1109/ISIE.2019.8781312.

[6] L. Tang and B.-T. Ooi, "Locating and isolating DC faults in multi-terminal DC systems," *IEEE Trans. Power Del.*, vol. 22, no. 3, pp. 1877–1884, Jul. 2007.

[7] M. E. Baran and N. R. Mahajan, "Overcurrent protection on VSC-based multi-terminal DC distribution systems," *IEEE Trans. Power Del.*, vol. 22, no. 1, pp. 406–412, 2007.

[8] Y. Song, J. Sun, M. Saeedifard, S. Ji, L. Zhu, and A. P. S. Meliopoulos, "Optimum selection of circuit breaker parameters based on analytical calculation of overcurrent and overvoltage in multiterminal HVDC grids," *IEEE Trans. Ind. Electron.*, vol. 67, no. 5, pp. 4133–4143, May 2020.

[9] J. Liu, N. Tai, and C. Fan, "Transient-Voltage-Based protection scheme for DC line faults in the multiterminal VSC-HVDC system," *IEEE Trans. Power Del.*, vol. 32, no. 3, pp. 1483–1494, Jun. 2017.

[10] R. Li, L. Xu, and L. Yao, "DC fault detection and location in meshed multiterminal HVDC systems based on DC reactor voltage change rate," *IEEE Trans. Power Del.*, vol. 32, no. 3, pp. 1516–1526, Jun. 2017.

[11] O. M. K. K. Nanayakkara, A. D. Rajapakse, and R. Wachal, "Location of DC line faults in conventional HVDC systems with segments of cables and overhead lines using terminal measurements," *IEEE Trans. Power Del.*, vol. 27, no. 1, pp. 279–288, Jan. 2012.

[12] D. Tzelepis, G. Fusiek, A. Dyśko, P. Niewczas, C. Booth, and X. Dong, "Novel fault location in MTDC grids with non-homogeneous transmission lines utilizing distributed current sensing technology," *IEEE Trans. Smart Grid*, vol. 9, no. 5, pp. 5432–5443, Sep. 2018, doi: 10.1109/TSG.2017.2764025.

[13] R. Nasr, O. Falou, A. Shahin, E. Hysi, L. A. Wirtzfeld, E. S. L. Berndl, and M. C. Kolios, "Mean scatterer spacing estimation using cepstrum-based continuous wavelet transform," *IEEE Trans. Ultrason., Ferroelectr., Freq. Control*, early access, Jan. 6, 2020, doi: 10.1109/TUFFC.2020.2963955.

[14] A. Raza, X. Dianguo, L. Yuchao, S. Xunwen, B. W. Williams, and C. Cecati, "Coordinated operation and control of VSC based multiterminal high voltage DC transmission systems," *IEEE Trans. Sustain. Energy*, vol. 7, no. 1, pp. 364–373, Jan. 2016.

[15] E. Kontos, R. T. Pinto, S. Rodrigues, and P. Bauer, "Impact of HVDC transmission system topology on multiterminal DC network faults," *IEEE Trans. Power Del.*, vol. 30, no. 2, pp. 844–852, Apr. 2015.

[16] W. Wang, M. Barnes, O. Marjanovic, and O. Cwikowski, "Impact of DC breaker systems on multiterminal VSC-HVDC stability," *IEEE Trans. Power Del.*, vol. 31, no. 2, pp. 769–779, Apr. 2016.

[17] F. Deng and Z. Chen, "Design of protective inductors for HVDC transmission line within DC grid offshore wind farms," *IEEE Trans. Power Del.*, vol. 28, no. 1, pp. 75–83, Jan. 2013.

[18] H. Livani and C. Y. Evrenosoglu, "A single-ended fault location method for segmented HVDC transmission line," *Electric Power Syst. Res.*, vol. 107, pp. 190–198, Feb. 2014.

[19] D. Tzelepis, "Single-ended differential protection in mtdc networks using optical sensors," *IEEE Trans. Power Del.*, vol. 32, no. 3, pp. 1605–1615, Jun. 2017.

[20] U. Amir Khan, J.-G. Lee, F. Amir, and B.-W. Lee, "A novel model of HVDC hybrid-type superconducting circuit breaker and its performance analysis for limiting and breaking DC fault currents," *IEEE Trans. Appl. Supercond.*, vol. 25, no. 6, Dec. 2015, Art. no. 5603009.

[21] L. Chen, G. Li, H. He, H. Chen, Y. Li, M. Ding, X. Zhang, Y. Xu, L. Ren, and Y. Tang, "Study on coordination of resistive SFCLs and hybrid-type circuit breakers to protect a HVDC system with LCC and VSC stations," *IEEE Trans. Appl. Supercond.*, vol. 30, no. 4, Jun. 2020, Art. no. 5600806.

[22] Martisen and Erik, "Evaluation of methods for detecting and locating faults in HVDC grids," M.S. thesis, Norwegian Univ. Sci. Technol., Trondheim, Norway, 2014.

[23] N. A. Belda and R. P. P. Smeets, "Test circuits for HVDC circuit breakers," *IEEE Trans. Power Del.*, vol. 32, no. 1, pp. 285–293, Feb. 2017.

[24] S.-M. Xue and C. Liu, "Line-to-Line fault analysis and location in a VSC-based low-voltage DC distribution network," *Energies*, vol. 11, no. 3, p. 536, 2018.

[25] R. Dantas, J. Liang, C. E. Ugalde-Loo, A. Adamczyk, C. Barker, and R. Whitehouse, "Progressive fault isolation and grid restoration strategy for MTDC networks," *IEEE Trans. Power Del.*, vol. 33, no. 2, pp. 909–918, Apr. 2018.

[26] X. Yu and L. Xiao, "A DC fault protection scheme for MMC-HVDC grids using new directional criterion," *IEEE Trans. Power Del.*, early access, Mar. 2, 2020, doi: 10.1109/TPWRD.2020.2977373.

RIFAT ARA (Student Member, IEEE) received the B.E. degree in electronics and communication engineering from Bangalore University, India, and the M.S. degree in electrical engineering from Mirpur University of Science and Technology (MUST), Pakistan, in 2009. She is currently pursuing the Ph.D. degree with the Department of Electrical Engineering, Capital University of Science and Technology, Pakistan. Since 2007, she has been a Senior Lecturer with the Departments of Electrical and Power Engineering, MUST. Her general research interests include HVDC protection schemes, smart grids, and fault detection algorithms.

UMER AMIR KHAN (Member, IEEE) was born in Karachi, Pakistan, in May 1984. He received the B.E. degree from the National University of Sciences & Technology, Islamabad, Pakistan, in 2006, and the M.S. and Ph.D. degrees from Hanyang University, Ansan, South Korea, in 2011 and 2016, respectively.

He was an Assistant Professor at NUST, Pakistan, until 2016. Since 2016, he has been with the Capital University of Sciences and Technology, Pakistan. His research interests include protection systems and switchgear design for HVDC systems, high-voltage power electronics, smart grid, and renewable energy systems.

Prof. Khan is a registered engineer at Pakistan Engineering Council and a member of Korean Institute of Electrical Engineers (KIEE) and the IEEE Power and Energy Society.

AAMIR IQBAL BHATTI (Senior Member, IEEE) received the M.S. degree in control systems from Imperial College London, London, U.K., in 1994, and the Ph.D. degree in control engineering from Leicester University, Leicester, U.K., in 1998. Since 2007, he has been a Professor with the Department of Electrical Engineering, Capital University of Science and Technology, Islamabad, Pakistan. He is currently the Pioneering Head of the Control and Signal Processing Research Group, CSPR, Pakistan. His research areas include GSR development, radar signals, line Echo canceller design, GSM audio codes, dynamic system modeling, and large diesel systems.

BANG WOOK LEE (Senior Member, IEEE) received the B.S., M.S., and Ph.D. degrees in electrical engineering from Hanyang University, Seoul, South Korea, in 1991, 1993, and 1998, respectively. He was a Senior Research Engineer with LS Industrial Systems Co., Ltd., South Korea. In 2008, he joined the Department of Electronic System Engineering, Hanyang University, Ansan, South Korea, where he is currently a Professor. His research interests include HVDC protection systems, high voltage insulation, renewable energies, and development of electrical equipment, including transmission line structures for HVDC and HVAC power systems. He is a member of HVDC Research Committee of the KIEE, of Power Cable Experts Committee of the Korean Agency for Technology and Standards, and CIGRE.

• • •